Herschel Search for O2 toward the Orion Bar

Melnick, Gary J.; Tolls, Volker; Goldsmith, Paul F.; Kaufman, Michael J.; Hollenbach, David J.; Black, John H.; Encrenaz, Pierre; Falgarone, Edith; Gerin, Maryvonne; Hjalmarson, Åke

Published in:
Astrophysical Journal

DOI:
10.1088/0004-637X/752/1/26

Publication date:
2012

The Astrophysical Journal, 752:26 (9pp), 2012 June 10 doi:10.1088/0004-637X/752/1/26

HERSCHEL SEARCH FOR O_2 TOWARD THE ORION BAR*

Gary J. Melnick[1], Volker Tolls[1], Paul F. Goldsmith[2], Michael J. Kaufman[3], David J. Hollenbach[4], John H. Black[5], Pierre Encrenaz[6], Edith Falgarone[7], Maryvonne Gerin[7], Åke Hjalmarson[5], Di Li[8], Dariusz C. Lis[9], René Liseau[5], David A. Neufeld[10], Laurent Pagani[6], Ronald L. Snell[11], Floris van der Tak[12], and Ewine F. van Dishoeck[13,14]
[1] Harvard-Smithsonian Center for Astrophysics, 60 Garden Street, MS 66, Cambridge, MA 02138, USA
[2] Jet Propulsion Laboratory, California Institute of Technology, 4800 Oak Grove Drive, Pasadena, CA 91109, USA
[3] Department of Physics and Astronomy, San Jośe State University, San Jose, CA 95192, USA
[4] SETI Institute, Mountain View, CA 94043, USA
[5] Department of Earth & Space Sciences, Chalmers University of Technology, Onsala Space Observatory, SE-439 92 Onsala, Sweden
[6] LERMA & UMR8112 du CNRS, Observatoire de Paris, 61 Av. de l'Observatoire, 75014 Paris, France
[7] LRA/LERMA, CNRS, UMR8112, Observatoire de Paris & École Normale Supérieure, 24 rue Lhomond, 75231 Paris Cedex 05, France
[8] National Astronomical Observatories, Chinese Academy of Sciences, A20 Datun Road, Chaoyang District, Beijing 100012, China
[9] California Institute of Technology, Cahill Center for Astronomy and Astrophysics 301-17, Pasadena, CA 91125, USA
[10] Department of Physics and Astronomy, Johns Hopkins University, 3400 North Charles Street, Baltimore, MD 21218, USA
[11] Department of Astronomy, University of Massachusetts, Amherst, MA 01003, USA
[12] SRON Netherlands Institute for Space Research, P.O. Box 800, 9700 AV, and Kapteyn Astronomical Institute, University of Groningen, Groningen, The Netherlands
[13] Leiden Observatory, Leiden University, P.O. Box 9513, 2300 RA, Leiden, The Netherlands
[14] Max-Planck-Institut für Extraterrestrische Physik, Giessenbachstrasse 1, 85748, Garching, Germany
Received 2012 February 14; accepted 2012 April 9; published 2012 May 23

ABSTRACT

We report the results of a search for molecular oxygen (O_2) toward the Orion Bar, a prominent photodissociation region at the southern edge of the H II region created by the luminous Trapezium stars. We observed the spectral region around the frequency of the O_2 $N_J = 3_3$–1_2 transition at 487 GHz and the 5_4–3_4 transition at 774 GHz using the Heterodyne Instrument for the Far-Infrared on the *Herschel Space Observatory*. Neither line was detected, but the 3σ upper limits established here translate to a total line-of-sight O_2 column density $<1.5 \times 10^{16}$ cm^{-2} for an emitting region whose temperature is between 30 K and 250 K, or $<1 \times 10^{16}$ cm^{-2} if the O_2 emitting region is primarily at a temperature of $\lesssim$100 K. Because the Orion Bar is oriented nearly edge-on relative to our line of sight, the observed column density is enhanced by a factor estimated to be between 4 and 20 relative to the face-on value. Our upper limits imply that the face-on O_2 column density is less than 4×10^{15} cm^{-2}, a value that is below, and possibly well below, model predictions for gas with a density of 10^4–10^5 cm^{-3} exposed to a far-ultraviolet flux 10^4 times the local value, conditions inferred from previous observations of the Orion Bar. The discrepancy might be resolved if (1) the adsorption energy of O atoms to ice is greater than 800 K; (2) the total face-on A_V of the Bar is less than required for O_2 to reach peak abundance; (3) the O_2 emission arises within dense clumps with a small beam filling factor; or (4) the face-on depth into the Bar where O_2 reaches its peak abundance, which is density dependent, corresponds to a sky position different from that sampled by our *Herschel* beams.

Key words: astrochemistry – ISM: abundances – ISM: individual objects (Orion) – ISM: molecules – submillimeter: ISM

Online-only material: color figures

1. INTRODUCTION

Searches for interstellar O_2 have a long history, but their motivation has evolved with time. Prior to the late 1990's, efforts to detect O_2 were driven largely by a desire to confirm its predicted role as a major reservoir of elemental oxygen within dense molecular clouds and as the most important gas coolant—after CO—of cold ($T \lesssim 30$ K), modestly dense ($n(H_2) \simeq 10^3$–10^4 cm^{-3}) gas (cf. Goldsmith & Langer 1978; Neufeld et al. 1995). The launch of the *Submillimeter Wave Astronomy Satellite (SWAS)* in 1998 and *Odin* in 2001, and the subsequent failure of these observatories to detect O_2 toward a large number of sources at levels of a few percent of the abundances predicted by equilibrium gas-phase chemical models, have forced a shift in emphasis to a re-examination of the oxygen chemistry in dense molecular gas. Today, interest in O_2 no longer lies in its being a significant reservoir of elemental oxygen or in its cooling power. Instead, because the abundance of gas-phase O_2 is set by a balance of various formation, destruction, and depletion processes thought to affect the broader chemistry in dense gas—such as gas-phase reactions, grain-surface reactions, thermal sublimation, far-ultraviolet (FUV) photodesorption, cosmic-ray desorption, photodissociation, and freeze out—measures of O_2 have become an important test of our current understanding of the relative effectiveness of these processes.

The capabilities of the *Herschel Space Observatory's* Heterodyne Instrument for the Far-Infrared (HIFI; de Graauw et al. 2010) have enabled improved searches for O_2 through (1) its high sensitivity, including at 487 GHz—the frequency of the $N_J = 3_3$–1_2 transition observed previously by *SWAS* and *Odin*; and (2) its broad frequency coverage that permits observations of additional O_2 submillimeter transitions, some of which are expected to exhibit stronger emission than the 3_3–1_2 line under certain physical conditions. The Open Time Key Program

* *Herschel* is an ESA space observatory with science instruments provided by European-led Principal Investigator consortia and with important participation from NASA.

"*Herschel* Oxygen Project" (HOP; Co-PIs P. Goldsmith and R. Liseau) is designed to survey Galactic sources with the goal to detect O_2 or set meaningful limits on its abundance within these regions. Because the effectiveness of the processes that determine the O_2 column density depends upon the gas density, temperature, and incident FUV flux G_o (scaling factor in multiples of the average Habing local interstellar radiation field; Habing 1968) among other parameters, testing these models requires that the HOP observations include a range of source types, such as dense quiescent clouds, outflows and shocked gas regions, and FUV-illuminated cloud surfaces (see, for example, Goldsmith et al. 2011; Liseau et al. 2012).

In this paper, we report the results of a deep search for O_2 emission toward the Orion Bar, a well-known ionization front located approximately 2′ southeast of the Trapezium stars in Orion at the interface of the H II region created by these stars and the dense gas associated with the surrounding Orion molecular cloud. The Orion Bar lends itself well to the study of FUV-illuminated molecular gas for several reasons, including its nearly edge-on geometry, its proximity (∼420 pc; Menten et al. 2007; Hirota et al. 2007; Kim et al. 2008), its relatively high density ($n(H_2) \gtrsim 3 \times 10^4$ cm^{-3}), and the strong ($G_o \simeq 10^4$–10^5) external FUV field irradiating this gas. The Orion Bar, and sources like it, are of particular interest since the dust grains within these regions are predicted to be sufficiently warm that the thermal evaporation of O atoms from the grain surfaces is enhanced, resulting in a higher fraction of O in the gas phase and the increased production of O_2 via gas-phase chemical reactions ($O + OH \rightarrow O_2 + H$). Under such circumstances, the O_2 column density can be more than a factor of 10 greater than within gas exposed to lower (i.e., $G_o < 500$) external FUV fields (cf. Hollenbach et al. 2009). The inclusion of the Orion Bar within the HOP program was intended to test this prediction.

The observations and data reduction methods are described in Section 2 below. In Section 3, we present the resultant spectra and the upper limits to the O_2 integrated intensity. In Section 4, we review the excitation conditions within the Orion Bar and the derived limits on the line-of-sight O_2 column density. In Section 5, we discuss these limits in the context of recent chemical models that trace the O_2 abundance from the FUV-illuminated cloud surface to the deep interior.

2. OBSERVATIONS AND DATA REDUCTION

The *Herschel*/HIFI observations presented here were carried out using the HIFI Band 1a receiver for the 3_3–1_2 487 GHz observations and the HIFI Band 2b receiver for the 5_4–3_4 774 GHz observations. The 487 GHz observations were conducted on operational day (OD) 291 in spectral scan dual beam switch (DBS) mode, while the 774 GHz observations were conducted on OD 297 in spectral scan DBS mode and on OD 509 in HIFI single-point DBS mode. Eight local oscillator (LO) settings were used for both the 487 GHz and 774 GHz spectral scans to enable the spectral deconvolution, and the additional eight single-point 774 GHz observations were observed also using eight different LO settings. The total integration time (on-source + off-source) *for each polarization* was 0.93 hr for the 487 GHz spectral scan, 0.86 hr for the 774 GHz spectral scan, and a total of 4.6 hr for the eight single-point 774 GHz observations. The FWHM beam sizes were 44.″7 at 487 GHz and 28.″2 at 774 GHz.

The observed position, $\alpha = 5^h35^m20.^s6$, $\delta = -5^\circ25'14.''0$ (J2000), is shown in Figure 1. We applied the total observing time allotted to HOP observations of the Orion Bar to a single spatial position—versus multiple positions—in order to achieve the lowest radiometric noise and, thus, the greatest sensitivity to weak O_2 emission. In the absence of prior information about the possible O_2 spatial distribution, our choice of sky position was guided by the desire to place the 487 GHz and 774 GHz beam centers a distance corresponding to approximately 8 visual magnitudes into the molecular gas measured from the ionization front, in accordance with model predictions (see Section 5 for a full discussion). For an H_2 density between 5×10^4 cm^{-3} and 5×10^5 cm^{-3}, applicable to the interclump medium in the Bar, and $G_o \simeq 10^4$, this corresponds to a projected angular distance of between 2.″4 and 24″ from the ionization front. As shown in Figure 1, the selected position places the beams in the center of this range, while the beam sizes encompass the full range. The sky position parallel to the Orion Bar was selected to coincide with the molecular gas, as delineated by the ^{13}CO $J = 3$–2 emission (see Figure 1), and, for future analysis, one of the positions under present study by another *Herschel* Key Program.

The data were processed using the standard HIFI pipeline software HIPE version 7.3 (Ott 2010), spurious signals (spurs) removed, spectra defringed, spectral scans deconvolved, and all data finally exported to GILDAS-CLASS format. Further processing was performed only on the Wide Band Spectrometer (WBS) spectra (0.5 MHz channel spacing and 1.1 MHz effective spectral resolution) using the IRAM GILDAS software package (http://iram.fr/IRAMFR/GILDAS/), including first-order baseline removal, averaging of the 774 GHz spectral scans and frequency-aligned single-point observations, averaging of the H- and V-polarization spectra, and production of separate averages for both frequencies and both sidebands. The frequencies for the line identification were extracted from the JPL and CDMS databases (Pickett et al. 1998; Müller et al. 2005) as well as Drouin et al. (2010) in the case of O_2.

3. RESULTS

A summary of the identified lines in the HIFI Band 1a and Band 2b spectra along with the observing modes, integration times, and Gaussian fit parameters is provided in Table 1. The summed H+V polarization spectra observed in Band 1a are shown in Figure 2, while those observed in Band 2b are shown in Figure 3. With the exception of the H_2Cl^+ chloronium 485 GHz spectrum, which is a blend of three hyperfine components (cf. Lis et al. 2010; Neufeld et al. 2012), all of the detected lines appear well fit by single Gaussian profiles with a common LSR line center of 10.68 ± 0.14 km s^{-1} (1σ) and individual best-fit FWHM line widths ranging from about 1.8 km s^{-1} to 2.5 km s^{-1}.

The upper limit to the integrated intensity of the O_2 3_3–1_2 and 5_4–3_4 transitions is derived assuming each line is described by a single Gaussian profile, as is the case for the other unblended lines we detect toward this position. The rms noise in the O_2 3_3–1_2 487 GHz spectrum between LSR velocities of −110 km s^{-1} and +25 km s^{-1}—a velocity range within which there is no evidence for any spectral features—is 2.62 mK per 0.5 MHz channel. Similarly, the rms noise in the O_2 5_4–3_4 774 GHz spectrum between LSR velocities of −70 km s^{-1} and +30 km s^{-1} is 2.19 mK per 0.5 MHz channel. The intrinsic O_2 line widths along this line of sight are unknown; however, we assume they lie between the extremes of 1.8 km s^{-1} and 2.5 km s^{-1} (FWHM) measured for the other unblended lines we detect along this line of sight (see Table 1). This leads to 3σ upper limits of between 0.0150 and 0.0209 K km s^{-1} for the 3_3–1_2 487 GHz line and between 0.0126 and 0.0175 K km s^{-1} for the 5_4–3_4 774 GHz line.

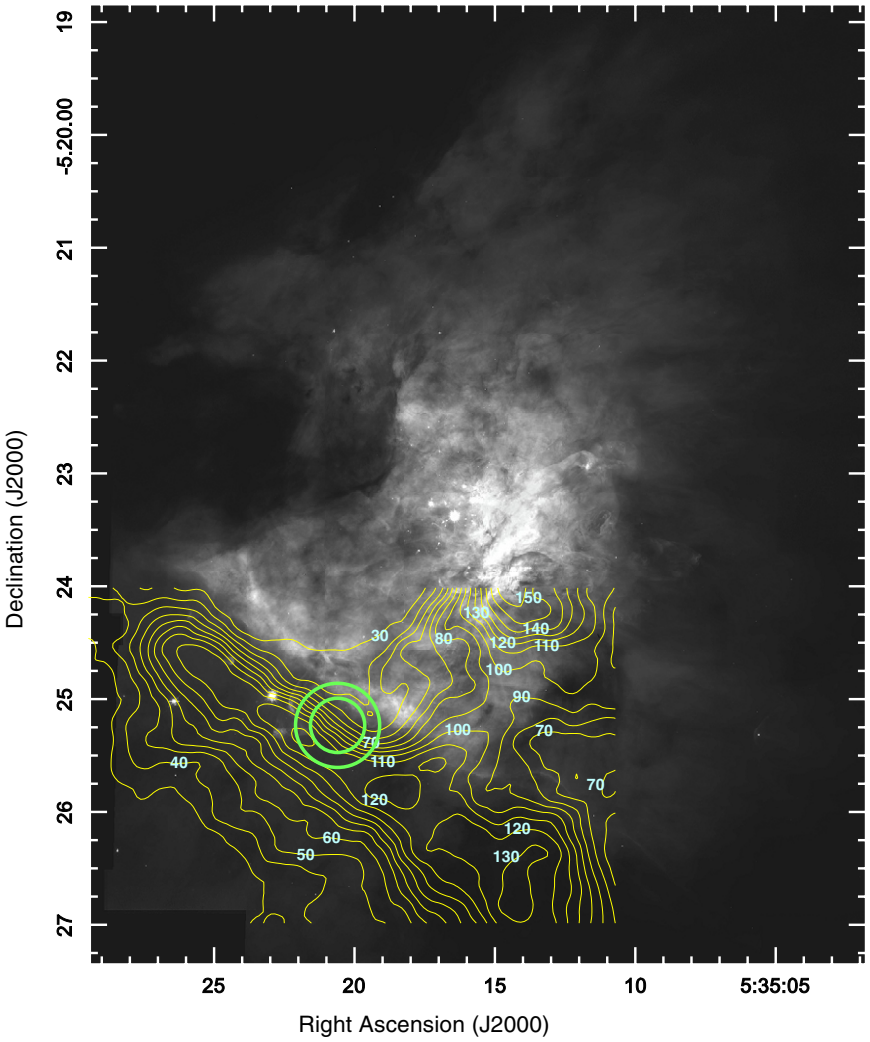

Figure 1. Position of the HIFI 44.″7 and 28.″2 beams at 487 GHz and 774 GHz, respectively, superposed on a *Hubble Space Telescope* image of the Orion Nebula (O'Dell & Wong 1996). Also shown are contours of ^{13}CO $J = 3$–2 integrated intensity for a portion of a larger map obtained by Lis & Schilke (2003), with intensities in K km s^{-1} noted. The HIFI beams are centered at $\alpha = 05^{h}35^{m}20.^{s}6$, $\delta = -05^{\circ}25'14''$ (J2000), toward the surface layers of the FUV-illuminated Orion Bar where the O_2 emission is predicted to peak.

(A color version of this figure is available in the online journal.)

4. EXCITATION AND LIMITS ON THE O_2 COLUMN DENSITY

The Orion Bar, like many other photodissociation regions (PDRs), displays emission from a variety of ionic, atomic, and molecular species best fit by a mix of gas densities and temperatures. The broad picture to emerge is that of a layer consisting of at least two components: interclump gas with $n(H_2) \sim 3$–20×10^4 cm^{-3} (Hogerheijde et al. 1995; Wyrowski et al. 1997; Simon et al. 1997; Marconi et al. 1998) surrounding clumps with $n(H_2) \sim 10^6$–10^7 cm^{-3} (Lis & Schilke 2003; Young Owl et al. 2000), which comprise about 10% of the mass (Jansen et al. 1995). Gas temperature estimates similarly vary, depending on the species observed and the component giving rise to most of the emission. Within the denser well-shielded gas, the gas temperature is thought to range between ~50 and 85 K (Hogerheijde et al. 1995; Gorti & Hollenbach 2002). The gas temperature associated with the interclump medium is estimated to be 85 ± 30 K (Hogerheijde et al. 1995), with some gas temperatures associated with the surfaces ($A_V \lesssim 1$) of the denser clumps ranging as high as 220 K (Jansen et al. 1995; Batrla & Wilson 2003; Goicoechea et al. 2011). There is evidence for an even warmer component (300–700 K) based on emission from pure rotational lines of H_2 and far-infrared fine-structure lines of [O I] at 63 and 145 μm and [C II] at 158 μm (Herrmann et al. 1997; Allers et al. 2005). This warmer component is believed to arise in the gas between the ionization front and the molecular region traced by ^{13}CO emission (Walmsley et al. 2000). The strength of the FUV field incident on the Orion Bar has been estimated to be $G_o \simeq 1$–4×10^4 based upon the total radiation from the Trapezium stars—and the O star θ^1 Ori C in particular—the intensity of the far-infrared [C II] and [O I] fine-structure lines mapped toward the Orion molecular ridge, the strength of several near-infrared lines whose intensities have been ascribed to recombinations to highly excited states of CI, and the strength of near-infrared N I lines excited by the fluorescence of UV lines (Herrmann et al. 1997; Marconi et al. 1998; Walmsley et al. 2000). Given a density of $\sim 10^5$ cm^{-3} for the bulk of the material and a G_o of $\sim 10^4$, models predict that the O_2 abundance peaks at $A_V \gtrsim 8$ mag. (cf. Sternberg & Dalgarno 1995; Hollenbach et al. 2009). At these depths into the cloud, the gas temperature is predicted to be 30–40 K

Table 1
Summary of Observations

Species	Transition	Rest Frequency[a] (GHz)	Observing Mode[b]	Integration Time (hr)	Gaussian Fit Parameters			
					T_A^* Amplitude (K)	LSR Line Center (km s^{-1})	FWHM (km s^{-1})	Integrated Intensity (K km s^{-1})
H_2Cl^+	$J = 1_{11}$–0_{00}							
	$F = 3/2$–$3/2$	485.413	sc	1.16	0.055	10.56	2.47	0.15
	$F = 5/2$–$3/2$	485.418	sc	1.16	0.076	10.56	2.47	0.20
	$F = 1/2$–$3/2$	485.421	sc	1.16	0.030	10.57	2.47	0.08
SO^+	$J = 21/2$–$19/2$ $\Omega = 1/2$, $\ell = e$	486.837	sc	1.85	0.029	10.77	2.28	0.07
SO^+	$J = 21/2$–$19/2$ $\Omega = 1/2$, $\ell = f$	487.212	sc	1.85	0.027	10.99	1.86	0.05
O_2	3_3–1_2	487.249	sc	1.85	$\leqslant$0.008[c]	...	...	...
CS	$J = 10$–9	489.751	sc	0.46	0.46	10.58	1.78	0.87
^{13}CO	$J = 7$–6	771.184	sp	1.15	27.04	10.67	2.24	64.48
O_2	5_4–3_4	773.840	sc, sp	10.91	$\leqslant$0.007[c]	...	...	...
C_2H	$N = 9$–8 $J = 19/2$–$17/2$ $F = 9$–8	785.802	sc, sp	10.91	0.34	10.76	2.35	0.84
C_2H	$N = 9$–8 $J = 17/2$–$15/2$ $F = 9$–8	785.865	sc, sp	10.91	0.30	10.77	2.35	0.75
$C^{17}O$	$J = 7$–6	786.281	sc, sp	10.91	1.19	10.62	1.76	2.23

Notes.
[a] NRAO-recommended rest frequency.
[b] sc: spectral scan observation; sp: single-point observation.
[c] 3σ upper limit.

(Hollenbach et al. 2009). Thus, in our analysis, we consider the possibility that the O_2 emission could arise in gas with temperatures anywhere between 30 K and 250 K.

The weak line flux of the O_2 magnetic dipole transitions makes them highly likely to be optically thin. Under the assumption that the O_2 emission uniformly fills the HIFI beam, the observed integrated intensity in a given transition is

$$\int T_{\rm mb}\, dv = \frac{hc^3}{8\pi \nu^2 k}\ A_{u\ell}\ N(O_2)\ f_u = 5.15 \times 10^{-4}\ \frac{A_{u\ell}\ N(O_2)\ f_u}{\nu^2_{\rm GHz}}\ ({\rm K\,km\,s^{-1}}), \quad (1)$$

where $T_{\rm mb}$ is the main beam temperature, ν is the line frequency (and $\nu_{\rm GHz}$ is the line frequency in GHz), $A_{u\ell}$ is the spontaneous decay rate between the transition upper level, u, and lower level, ℓ, $N(O_2)$ is the total O_2 column density in cm^{-2}, and f_u is the fractional population in the transition upper level. The conversion between main beam and antenna temperature makes use of the efficiencies reported in Roelfsema et al. (2012).

To determine the fractional population of the transition upper state, f_u, the excitation of the lowest 36 levels of O_2, corresponding to a maximum upper-level temperature of 1141 K, was computed under the large velocity gradient (LVG) approximation. The spontaneous decay rates are those of Drouin et al. (2010) and the collisional rate coefficients are those calculated by Lique (2010) for He–O_2 collisions, multiplied by 1.37 to account for the different reduced mass when H_2 is the collision partner. For molecular hydrogen densities $>3 \times 10^4$ cm^{-3}, both the 3_3–1_2 and 5_4–3_4 transitions are close to (or in) LTE and the values of f_u depend essentially only on the temperature. Figure 4 shows the resulting contours of integrated antenna temperature for the 3_3–1_2 transition as functions of the total O_2 column density and gas temperature between 30 and 250 K. Similarly, Figure 5 shows the corresponding results for the 5_4–3_4 transition.

Of the two O_2 lines searched for here, an examination of Figures 4 and 5 shows that our measured upper limits to the 5_4–3_4 774 GHz integrated intensity place a more stringent limit on the maximum O_2 column density for $T_{\rm gas} > 35$ K (and comparable limits to that set by the 487 GHz line at $T_{\rm gas} \sim 30$ K). Specifically, assuming the emission fills the beam, the total line-of-sight O_2 column density must be less than 1.5×10^{16} cm^{-2} (3σ). If the O_2 abundance peaks within the cooler well-shielded gas, for which $T_{\rm gas} \lesssim 100$ K, the upper limit to the total O_2 column density is less than 1×10^{16} cm^{-2} (3σ).

5. DISCUSSION

O_2 is produced primarily through the gas-phase reaction $O + OH \rightarrow O_2 + H$ and is destroyed by photodissociation for the cloud depths of interest here. Thus, the O_2 abundance is expected to peak where the FUV field has been heavily attenuated and where both the gas-phase O and OH abundances are high, which, in externally FUV-illuminated clouds, is predicted to occur within a relatively narrow (i.e., a few A_V deep) zone centered at an $A_V \lesssim 9$ mag from the cloud surface (cf. Hollenbach et al. 2009). The proximity of this zone to the surface and the range of depths over which the peak abundance occurs are governed by several important processes. Near the cloud surface, where the FUV field is largely unattenuated, the equilibrium O_2 abundance is low owing to a high photodissociation rate. Beyond a few A_V into the cloud, the FUV field is attenuated, the photodissociation rate reduced, and a region of peak O_2 (and H_2O) abundance is attained.

Within most clouds with $G_o < 500$, the path to O_2 formation is believed to start with the formation of water ice, $H_2O_{\rm ice}$,

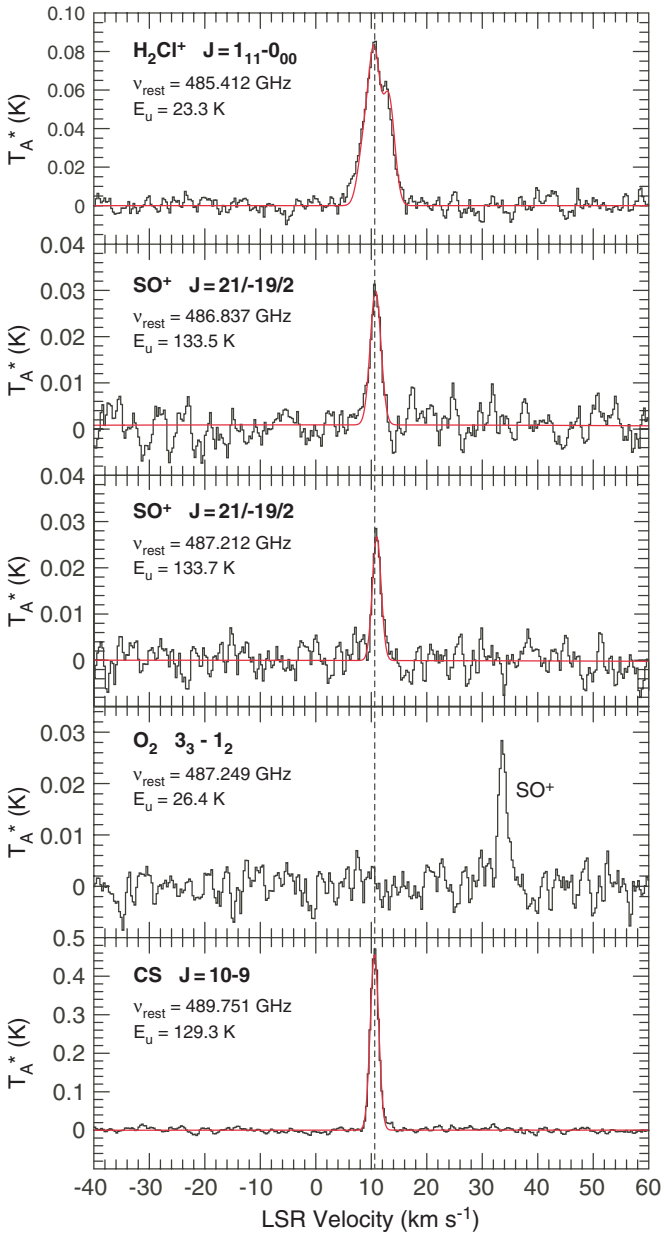

Figure 2. Averaged H- and V-polarization spectra obtained in HIFI Band 1a toward the Orion Bar, ordered by rest frequency, with the Gaussian fits given in Table 1 superposed in red. Also indicated is the energy of the upper level for each transition, in kelvin. The H_2Cl^+ line is a blend of three, partially resolved, hyperfine components (see Table 1). An LSR velocity of 10.7 km s^{-1} is denoted with a vertical dashed line.

(A color version of this figure is available in the online journal.)

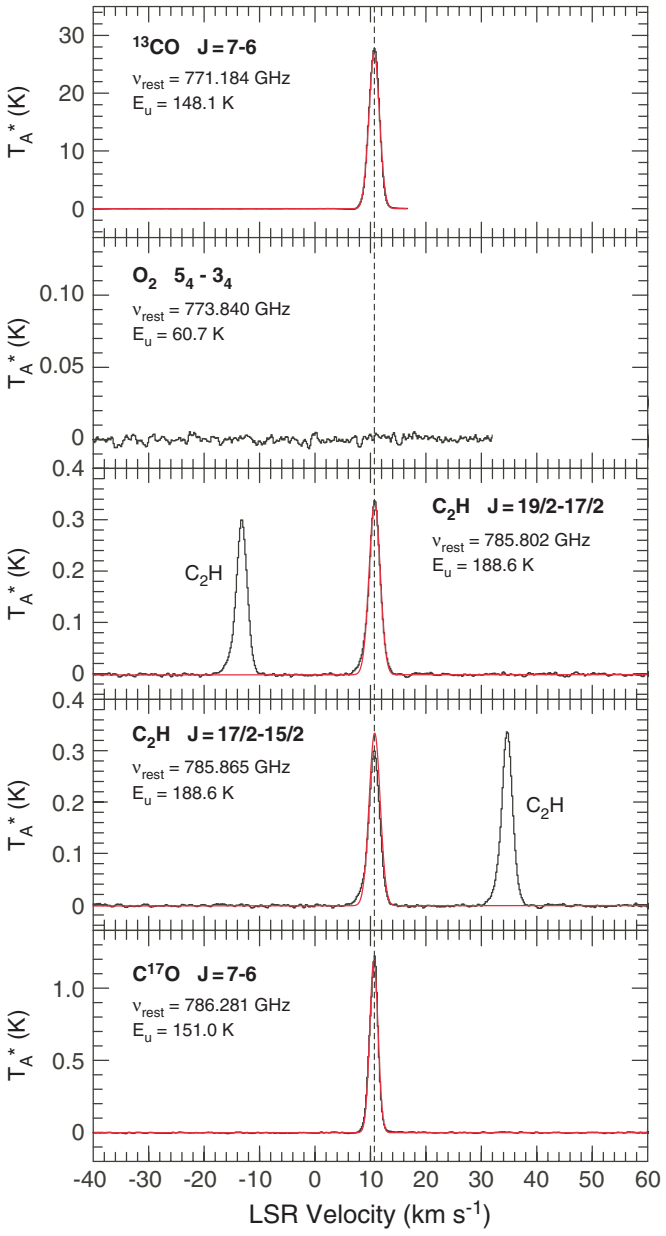

Figure 3. Averaged H- and V-polarization spectra obtained in HIFI Band 2b toward the Orion Bar, ordered by rest frequency, with the Gaussian fits given in Table 1 superposed in red. Also indicated is the energy of the upper level for each transition, in kelvin. An LSR velocity of 10.7 km s^{-1} is denoted with a vertical dashed line. The frequency of the ^{13}CO $J = 7$–6 transition was near the edge of the band and, thus, the spectrum does not cover the full LSR velocity range of the other lines. The O_2 spectrum has been truncated to remove features in the other sideband.

(A color version of this figure is available in the online journal.)

on grains, which occurs when O atoms strike and stick to grains long enough to combine with an accreted H atom to form OH_{ice} and then H_2O_{ice}. Within this region the FUV field remains strong enough to photodesorb H_2O from the ice mantles and subsequently photodissociate these molecules, creating sufficient gas-phase O and OH to produce O_2 by the gas-phase chemical reaction above. Deeper into the cloud (i.e., greater A_V), the FUV field is almost completely attenuated and the gas-phase OH and H_2O produced through the photodesorption and photodissociation of H_2O_{ice} drops significantly; most O atoms that then strike dust grains and form H_2O_{ice} remain locked in ice as long as the grain temperature is $\lesssim$100 K. Over time ($\sim 10^5$ years), this process greatly reduces the gas-phase atomic oxygen abundance and suppresses the formation and abundance of O_2. Hence, in the model of Hollenbach et al. (2009), the steady-state abundance profile of O_2 (and H_2O) resembles an elevated plateau that peaks at an $A_V \lesssim 6$ for gas with $n(H_2) = 10^4$–10^5 cm^{-3} and $G_o \lesssim 500$.

For regions subject to a G_o greater than $\sim$500, such as the Orion Bar, the scenario above is altered and, for several reasons, the peak O_2 abundance is higher and occurs at a higher A_V. First, the high FUV field absorbed at the cloud surface leads to a high infrared field that keeps the grains warm, even deep within the cloud. For $G_o = 10^4$, $T_{gr} \approx 40$ K to $A_V \gtrsim 8$,

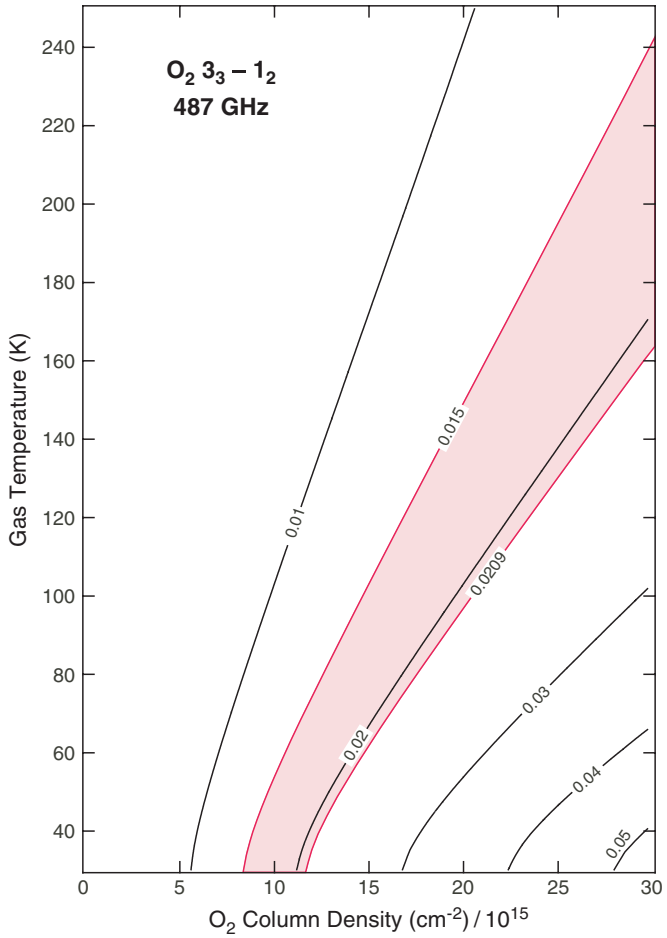

Figure 4. Contours of integrated antenna temperature, in K km s^{-1}, under a Gaussian line profile vs. line-of-sight O_2 column density and gas temperature assuming an aperture efficiency of 0.7. The shaded area bounds the range of upper limits to the O_2 487 GHz integrated intensity assuming the intrinsic O_2 line FWHM is 1.8 km s^{-1} (0.0150 K km s^{-1}) or 2.5 km s^{-1} (0.0209 K km s^{-1}).
(A color version of this figure is available in the online journal.)

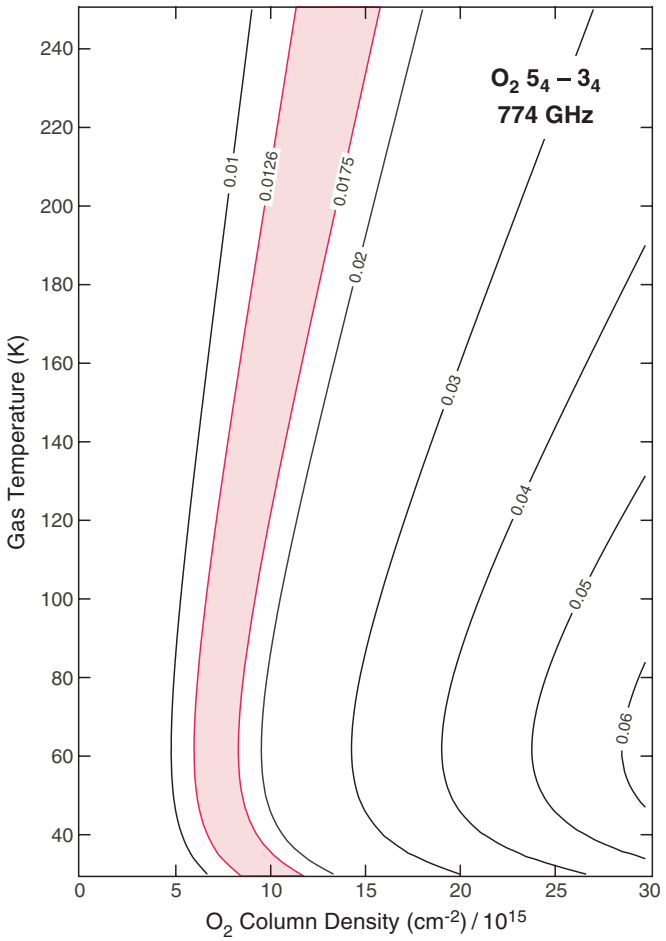

Figure 5. Contours of integrated antenna temperature, in K km s^{-1}, under a Gaussian line profile vs. line-of-sight O_2 column density and gas temperature assuming an aperture efficiency of 0.7. The shaded area bounds the range of upper limits to the O_2 774 GHz integrated intensity assuming the intrinsic O_2 line FWHM is 1.8 km s^{-1} (0.0126 K km s^{-1}) or 2.5 km s^{-1} (0.0175 K km s^{-1}).
(A color version of this figure is available in the online journal.)

resulting in a significant fraction of the O atoms being thermally desorbed from the grains before they can form H_2O_{ice} and leading to an increase in O in the gas phase. Second, the higher grain temperature also reduces the freeze out of such oxygen-bearing species as OH and O_2, further increasing the amount of elemental O in the gas phase. Finally, the attenuated FUV flux at the higher values of A_V lowers the photodestruction rates, allowing O_2 to survive to greater cloud depths. The combined result of these effects is a peak O_2 abundance about 3 times higher, and a total O_2 column density more than 10 times greater than for comparably dense gas exposed to $G_o \lesssim 500$. This result is reflected in the detailed calculations presented in Hollenbach et al. (2009) and shown in Figure 6, which is adapted from their paper. For this reason, the Orion Bar was considered a promising source for our attempts to detect O_2 emission.

From Figure 6, it would appear that the upper limits on the total O_2 column density established here are not in serious disagreement with the model predictions. However, the results shown in Figure 6 apply to a gas column perpendicular to the face of a planar cloud. This is not the geometry of the Orion Bar, which has often been described as an edge-on PDR, though its true structure has been the subject of some study and debate. For example, based on millimeter and submillimeter line observations, Hogerheijde et al. (1995) and Jansen et al. (1995) propose a model in which the Bar has a tilt angle, α, of $\sim 3^\circ$ from edge-on, resulting in an increase in the line-of-sight column density (beyond what would be measured for a face-on geometry) by a factor of $(\sin\alpha)^{-1}$, or almost 20. Alternately, Walmsley et al. (2000) find that a cylindrical model, in which the axis is in the plane of sky and the radius is 0.3 pc, best reproduces the observed spatial distribution of the fluorescent O I 1.317 μm emission. In this scenario, the average geometrical enhancement of the line-of-sight depth into the Bar versus the face-on depth is about 5. Finally, Neufeld et al. (2006) find that a geometrical enhancement factor of ~ 4 is required to reconcile observed and predicted C^+ column densities.

The 3σ upper limit to the *face-on* O_2 column density can thus be inferred from our line-of-sight values to be $1.5 \times 10^{16} \sin\alpha$ cm^{-2}, or $1.0 \times 10^{16} \sin\alpha$ cm^{-2} for $T_{gas} \lesssim 100$ K. (We note that these upper limits are derived assuming the intrinsic O_2 FWHM line width is 2.5 km s^{-1}; if the intrinsic width is closer to the lower end of the observed range, i.e., 1.8 km s^{-1}, the face-on O_2 column density upper limits are further reduced by a factor of 1.4.) For gas densities $\lesssim 10^5$ cm^{-3}, which applies to most of the gas in the Bar, this is to be compared with a total predicted face-on O_2 column density of $\gtrsim 7 \times 10^{15}$ cm^{-2}, as shown in Figure 6, with most of this column occurring inside a layer of peak O_2 abundance with a width corresponding

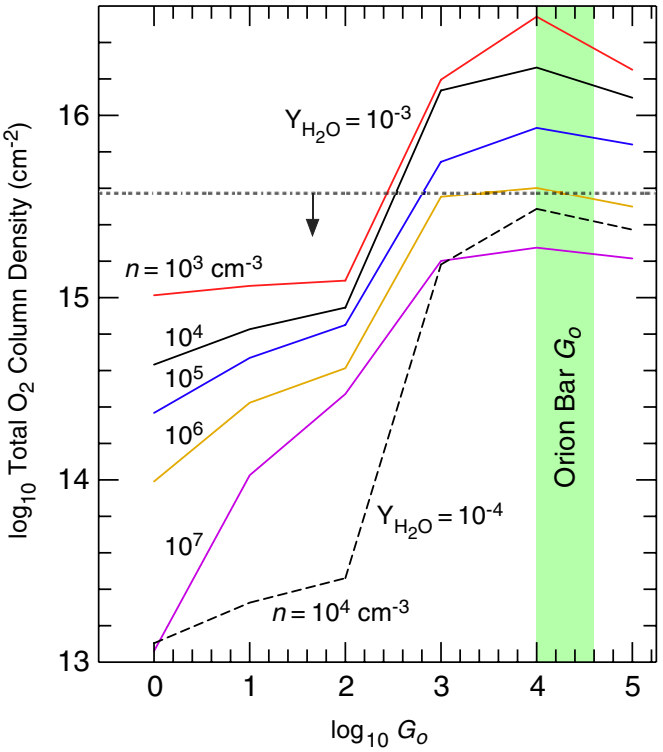

Figure 6. Predicted total O_2 column density perpendicular to the ionization front as a function of G_o and n(H+2H$_2$) for H_2O photodesorption yields of 10^{-3} (solid lines) and 10^{-4} (dashed line). The results shown assume a cloud thickness sufficient to encompass the zone of peak abundance (after Hollenbach et al. 2009). The range of G_o that applies to the Orion Bar is shown in the shaded region. The horizontal dotted line denotes the upper limit to the O_2 column density established here, i.e., 1.5×10^{16} cm^{-2}, divided by a geometrical enhancement factor of four.

(A color version of this figure is available in the online journal.)

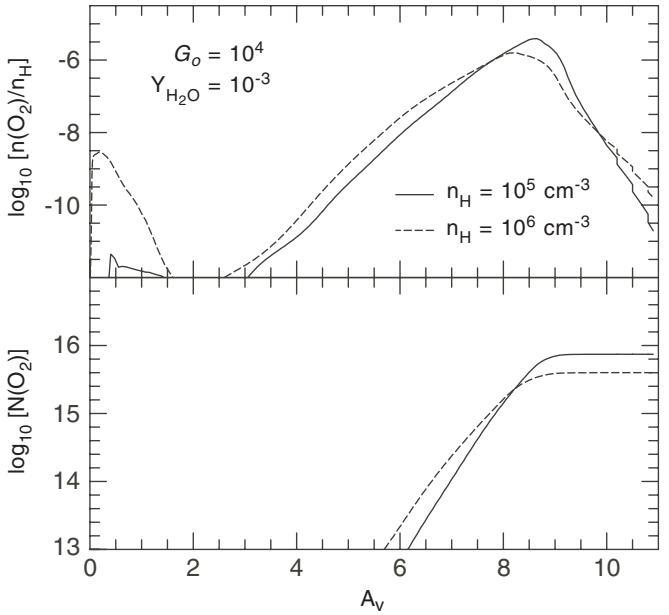

Figure 7. Top panel: abundance of O_2 as a function of face-on depth into a cloud, measured in A_V, for a cloud with $n_H = n(H + 2H_2) = 10^5$ cm^{-3} and 10^6 cm^{-3} exposed to an FUV field of $G_o = 10^4$. This result was computed using the model described in Hollenbach et al. (2009) assuming their "standard" model parameters, except for those noted here. An H_2O photodesorption yield of 10^{-3} is assumed. The gas and dust temperatures throughout the cloud are calculated self-consistently in the Hollenbach et al. code, which predicts a gas temperature of 33 K and a dust temperature of 42 K, at the depth of the peak O_2 abundance above. Bottom panel: cumulative face-on column density of O_2 integrated from the cloud surface to a given depth, in A_V, for the abundance profile shown in the top panel.

to approximately 2 mag (see Figure 7), or a linear size of $\sim 1.9 \times 10^{16}/n_5$ cm, where $n_5 = n(H_2)/[10^5$ cm$^{-3}]$. Viewed from a distance of 420 pc, this zone of peak O_2 emission would subtend $3[(1/n_5 + 162.4\ell \sin\alpha]''$, where ℓ is the physical length of the Bar in parsecs. For $\ell \simeq 0.6$ pc (cf. Jansen et al. 1995) and $n_5 \simeq 1$, $\alpha \gtrsim 6°$ would result in O_2 emission that fills the *Herschel*/HIFI beam at 774 GHz, though a minimum geometric enhancement factor of four, derived from other observations, suggests that α does not exceed 15°. However, these tilt angles imply an upper limit to the face-on O_2 column density between 1.6×10^{15} cm^{-2} and 3.9×10^{15} cm^{-2}, which is below, and in some cases significantly below, that predicted by theory.

For $\ell \simeq 0.6$ pc and $n_5 \simeq 1$, but $\alpha < 6°$, the O_2 layer no longer fills the 774 GHz beam. Although the peak O_2 column density within the beam will continue to increase for angles less than 6°, the beam filling factor will decrease. These two effects offset exactly, and the beam-averaged O_2 column density will remain the same for all tilt angles less than about 6°. Since the O_2 emission is optically thin, the line emission will likewise remain constant within the underfilled beam. In this case, the geometrical enhancement factor would be ~10, and the upper limit to the face-on O_2 column density remains below that predicted. Therefore, we conclude that Bar geometry cannot account for the discrepancy between theory and observations.

What, then, can account for the discrepancy? The amount of O_2 produced in externally FUV-illuminated dense gas depends on several factors, which we examine below:

Thermal evaporation. As noted earlier, the dwell time of an O atom on a grain surface can have a considerable effect on the O_2 abundance, particularly when this time becomes less than the time to combine with an H atom on the surface. The timescale for thermal evaporation of an O atom is approximately $9 \times 10^{-13} \exp[800\,\mathrm{K}/T_{gr}]$ s, where 800 K is the adsorption energy of O to water ice (Hasegawa & Herbst 1993) that applies to van der Waals binding to a chemically saturated surface. It is possible that the binding energy is greater than 800 K, which would increase the grain temperature, and thus the G_o, required to thermally desorb O atoms on short timescales and produce the jump in the total O_2 column density for $G_o \gtrsim 500$ seen in Figure 6. If, for example, the O adsorption energy was 1600 K, grains as warm as ~42 K—the expected dust temperature at high A_V in a $G_o \simeq 10^4$ field—would, on average, retain their O atoms long enough to form H_2O_{ice}, thus delaying the $G_o > 500$ rise in O_2 column density seen in Figure 6 until $G_o > 10^4$.

Photodesorption yield of H_2O from a grain surface, Y_{H_2O}. The abundance (and column density) of O_2 depends on the gas-phase abundance of O and OH, the latter being produced primarily through the photodissociation of H_2O, much of which is either photodesorbed from grains or produced via the dissociative recombination of gas-phase H_3O^+. At high G_o (and $T_{gr} > 20$ K), short O-atom dwell times on grains suppress the formation of OH_{ice} and H_2O_{ice}. However, even though it is not formed on the grain surface in a high-G_o environment, H_2O formed in the gas phase via H_3O^+ dissociative recombination will be depleted through freeze out onto grains and will remain locked in H_2O_{ice} for as long as $T_{gr} \lesssim 100$ K. Since the quantity of OH and H_2O returned to the gas phase as a consequence of H_2O_{ice}

photodesorption scales with Y_{H_2O}, the total O_2 column density likewise scales with Y_{H_2O}, as is seen in Figure 6. A value for Y_{H_2O} less than 10^{-3} would help to reconcile theory and observation. However, fits to the *SWAS* and *Odin* H_2O data (Hollenbach et al. 2009) as well as theoretical simulations and laboratory measurements (Andersson & van Dishoeck 2008; Arasa et al. 2011; Westley et al. 1995a, 1995b; Öberg et al. 2009) suggest, if anything, that the appropriate value of Y_{H_2O} is greater than 10^{-3}.

Grain cross-sectional area (per H). The equilibrium O_2 abundance in the A_V range of maximum O_2 abundance scales as $(Y_{H_2O})^2\,\sigma_H$, where σ_H is the grain cross-sectional area per H nucleus. Therefore, lowering σ_H will decrease the O_2 column density, bringing model and observation into closer agreement. For an "MRN" (Mathis et al. 1977) grain size distribution $n_{gr}(a) \propto a^{-3.5}$, where a is the grain radius, $\sigma_H \sim 2 \times 10^{-21}$ cm^2 for an assumed gas-to-dust mass ratio of 100 with grains ranging in radii between a minimum, a_{min}, of 20 Å and a maximum, a_{max}, of 2500 Å (the standard value in Hollenbach et al. 2009). Grains with $a_{min} < 20$ Å will be cleared of ice mantles by single photon heating or cosmic rays and, thus, are not significant ice reservoirs. Because $\sigma_H \propto (a_{min} \cdot a_{max})^{-0.5}$, in order to lower the value of σ_H while preserving the total mass in grains, either or both a_{min} and a_{max} must *increase*, such as through coagulation. For example, a reduction in σ_H, and thus the face-on O_2 column density, by at least a factor of two could be achieved if the minimum grain radius were to increase to $\gtrsim$80 Å.

Alternately, the buildup of an ice mantle, which can increase the radius of grains by as much as ∼50 Å, will increase the value of σ_H. For values of G_o of $\sim 10^4$ applicable to the Orion Bar, grain temperatures are expected to be ∼40 K, which is high enough to inhibit ice formation via surface reactions (absent a higher O adsorption energy); however, water formed in the gas phase via the reaction $H_3O^+ + e^- \rightarrow H_2O + H$ can still freeze out and form an ice mantle. Toward Orion, there is evidence for a departure from the assumed gas-to-dust mass ratio of 100, which is consistent with the buildup of ice mantles (see, for example, Goldsmith et al. 1997). In addition, there is evidence for a deficiency in small grains and for grain growth, possibly due to radiation pressure, the preferential evaporation of small grains, and coagulation (e.g., Cesarsky et al. 2000; Pellegrini et al. 2009; Shaw et al. 2009). The net effect of lowering σ_H through these processes, and increasing σ_H through the accumulation of an ice mantle, is unclear in a high-G_o environment like the Orion Bar.

Beam position. For an interclump H_2 density between 5×10^4 cm^{-3} and 5×10^5 cm^{-3} and $G_o = 10^4$, the peak O_2 abundance is predicted to occur at a face-on depth into the cloud corresponding to an $A_V \sim 8$ (see Figure 7). Thus, the linear distance from the $A_V = 0$ surface, which we assume is the prominent ionization front, to the depth of peak O_2 abundance is $\sim 7.6 \times 10^{21}/n(H_2)$ cm. For an assumed distance of 420 pc, the angular separation between the ionization front and the position of peak O_2 abundance (and column density) is then $\simeq 1.5\ A_V/[n(H_2)/10^5]$ arcsec, where A_V is the face-on depth of the O_2 peak abundance in magnitudes. Thus, an interclump H_2 density of 10^5 cm^{-3} should produce O_2 emission that peaks ∼12″ from the ionization front and close to the center of the observed sky positions (see Figure 1). However, if the interclump density is more than a factor of two different from 10^5 cm^{-3}—values that remain within the range of density estimates for the interclump medium—then the peak O_2 abundance is predicted to fall to either side of the observed beam center position.

Finally, we note that the inferred *peak* line-of-sight H_2 column density, $N(H_2)$, applicable to the interclump medium toward the Orion Bar is estimated to be 6.5×10^{22} cm^{-2} (Hogerheijde et al. 1995). If the geometrical enhancement factor is $\gtrsim$10, as would be the case for a tilt angle $\lesssim$5.5°, this would imply a face-on H_2 column density of $\lesssim 6.5 \times 10^{21}$ cm^{-2}, corresponding to a total A_V through the Bar of about 7. If the face-on extinction through the Orion Bar is indeed this low, then the attenuation of the $G_o \sim 10^4$ field is not sufficient to allow O_2 to reach its peak abundance and the total O_2 column density will be less than predicted by Hollenbach et al. (2009), whose total column densities are based upon cloud depths corresponding to $A_V \geqslant 10$. This is illustrated in Figure 7, which shows both the profile of O_2 abundance versus A_V and the cumulative O_2 column density to a given A_V, computed using the model described in Hollenbach et al. (2009) for the conditions appropriate to the Bar interclump medium. At a depth corresponding to an A_V of 7, the predicted face-on O_2 column density remains $<3 \times 10^{14}$ cm^{-2}, well below the limits set here.

The clumps known to exist within the Bar do possess higher H_2 densities (i.e., 10^6–10^7 cm^{-3}) and column densities (i.e., $>10^{23}$ cm^{-2}; Lis & Schilke 2003) and would provide the necessary FUV shielding to allow O_2 to reach its full predicted abundance. Such conditions help to reconcile observation and theory in two ways. First, as shown in Figure 6, the predicted total O_2 column densities *decrease* with higher H_2 densities. Thus, the total O_2 column density is predicted to be lower if the O_2 emission arises primarily from within the dense clumps rather than the surrounding lower density interclump medium. Second, interferometric observations indicate that the dense clumps within the Bar typically subtend angles of between 4″ and 8″ (see, for example, Lis & Schilke 2003), and thus provide a natural explanation for why the beam filling factor of O_2 emission could be less than unity. However, whether the correct explanation for what we observe is that O_2 emission originates preferentially within the dense clumps, and is suppressed within the $A_V \lesssim 7$ interclump medium, and with both gas components governed by the processes described in Hollenbach et al. (2009), will depend on how well this model reproduces the wealth of new lines being detected toward the Orion Bar by *Herschel*.

6. SUMMARY

1. We have conducted a search for O_2 toward the Orion Bar, carrying out deep integrations around the frequencies of the $N_J = 3_3$–1_2 and 5_4–3_4 transitions at 487 GHz and 774 GHz, respectively. Neither line was detected, but sufficiently sensitive limits on their integrated intensities were obtained to test current models of molecular gas exposed to high fluxes of FUV radiation—i.e., $G_o \sim 10^4$. In particular, we infer a total face-on O_2 column density of $\lesssim 4 \times 10^{15}$ cm^{-2}, assuming a Bar geometry in which the line-of-sight depth is more than four times greater than its face-on dimension. This column density is at least two times less than that predicted by the model of Hollenbach et al. (2009) for the densities, temperatures, and G_o appropriate to the Orion Bar.
2. The discrepancy between the model predictions and our observations would be reduced, if not eliminated, if the adsorption energy of atomic oxygen to water ice were greater than 800 K, and possibly as high as 1600 K. A lower value for the photodesorption yield for H_2O would help, but is not supported by fits to other astronomical data or recent theoretical calculations and laboratory measurements. A lower grain cross-sectional area per H, such as might

occur through grain coagulation, radiation pressure, or the preferential destruction of small grains, would lower the O_2 column density, but it is unclear whether these grain properties apply within the Orion Bar.

3. If the total face-on depth of the interclump medium within the Orion Bar corresponds to an $A_V \lesssim 7$, then photodissociation will reduce the O_2 column density to values below our detection limit. Clumps embedded within the Bar would offer sufficient shielding to enable the buildup of higher O_2 abundances and column densities in accord with model predictions, while the small filling factor of these clumps would reduce the O_2 line flux to levels consistent with our upper limits.
4. If the total face-on depth of the interclump medium within the Orion Bar corresponds to an $A_V > 8$, it remains possible that most of the O_2 emission may have been missed. In particular, since the gas density affects the angular separation between the ionization front and the face-on depth into the Bar at which the O_2 abundance is predicted to peak, interclump H_2 densities much different than the assumed value of 10^5 cm^{-3} could result in the position of peak O_2 abundance and column density occurring to either the northwest or southeast of the position we selected.

Only further modeling, including predictions for other species, can establish which, if any, of the above possibilities is most likely to resolve the present puzzle.

HIFI has been designed and built by a consortium of institutes and university departments from across Europe, Canada, and the United States under the leadership of SRON Netherlands Institute for Space Research, Groningen, The Netherlands, and with major contributions from Germany, France, and the United States. Consortium members are: Canada: CSA, U. Waterloo; France: CESR, LAB, LERMA, IRAM; Germany: KOSMA, MPIfR, MPS; Ireland, NUI Maynooth; Italy: ASI, IFSI-INAF, Osservatorio Astrofisico di Arcetri-INAF; Netherlands: SRON, TUD; Poland: CAMK, CBK; Spain: Observatorio Astronómico Nacional (IGN), Centro de Astrobiologá (CSIC-INTA). Sweden: Chalmers University of Technology - MC2, RSS & GARD; Onsala Space Observatory; Swedish National Space Board, Stockholm University–Stockholm Observatory; Switzerland: ETH Zurich, FHNW; USA: Caltech, JPL, NHSC. We also acknowledge the effort that went into making critical spectroscopic data available through the Jet Propulsion Laboratory Molecular Spectroscopy Data Base (http://spec.jpl.nasa.gov/), the Cologne Database for Molecular Spectroscopy (http://www.astro.uni-koeln.de/cdms/ and Müller et al. 2005), and the Leiden Atomic and Molecular Database (http://www.strw.leidenuniv.nl/∼moldata/ and Schöier et al. 2005). Finally, it is a pleasure to acknowledge useful discussions with Dr. Edwin Bergin.

Support for this work was provided by NASA through an award issued by JPL/Caltech.

REFERENCES

Allers, K. N., Jaffe, D. T., Lacy, J. H., Draine, B. T., & Richter, M. J. 2005, ApJ, 630, 368
Andersson, S., & van Dishoeck, E. F. 2008, A&A, 491, 907
Arasa, C., Andersson, S., Cuppen, H. M., van Dishoeck, E. F., & Kroes, G. J. 2011, J. Chem. Phys., 134, 164503
Batrla, W., & Wilson, T. L. 2003, A&A, 408, 231
Cesarsky, D., Jones, A. P., Lequeux, J., & Verstraete, L. 2000, A&A, 358, 708
de Graauw, T., Helmich, F. P., Phillips, T. G., et al. 2010, A&A, 518, L6
Drouin, B. J., Yu, S., Miller, C. E., et al. 2010, J. Quant. Spectrosc. Radiat. Transfer, 111, 1167
Goicoechea, J. R., Joblin, C., Contursi, A., et al. 2011, A&A, 530, L16
Goldsmith, P. F., Bergin, E. A., & Lis, D. C. 1997, ApJ, 491, 615
Goldsmith, P. F., & Langer, W. D. 1978, ApJ, 222, 881
Goldsmith, P. F., Liseau, R., Bell, T. A., et al. 2011, ApJ, 737, 96
Gorti, U., & Hollenbach, D. J. 2002, ApJ, 573, 215
Habing, H. J. 1968, Bull. Astron. Inst. Neth., 19, 421
Hasegawa, T. I., & Herbst, E. 1993, MNRAS, 261, 83
Herrmann, F., Madden, S. D., Nikola, T., et al. 1997, ApJ, 481, 343
Hirota, T., Bushimata, T., Choi, Y. K., et al. 2007, PASJ, 59, 897
Hogerheijde, M. R., Jansen, D. J., & Van Dishoeck, E. F. 1995, A&A, 294, 792
Hollenbach, D. J., Kaufman, M. J., Bergin, E. A., & Melnick, G. J. 2009, ApJ, 690, 1497
Jansen, D. J., Spaans, M., Hogerheijde, M. R., & Van Dishoeck, E. F. 1995, A&A, 303, 541
Kim, M. K., Hirota, T., Honma, M., et al. 2008, PASJ, 60, 991
Lique, F. 2010, J. Chem. Phys., 132, 044311
Lis, D. C., Pearson, J. C., Neufeld, D. A., et al. 2010, A&A, 521, L9
Lis, D. C., & Schilke, P. 2003, ApJ, 597, L145
Liseau, R., Goldsmith, P. F., Larsson, B., et al. 2012, A&A, submitted
Marconi, A., Testi, L., Natta, A., & Walmsley, C. M. 1998, A&A, 330, 696
Mathis, J. S., Rumpl, W., & Nordsieck, K. H. 1977, ApJ, 217, 425
Menten, K. M., Reid, M. J., Forbrich, J., & Brunthaler, A. 2007, A&A, 474, 515
Müller, H. S. P., Schöder, F., Stutzki, J., & Winnewisser, G. 2005, J. Mol. Struct., 742, 215
Neufeld, D. A., Lepp, S., & Melnick, G. J. 1995, ApJS, 100, 132
Neufeld, D. A., Roueff, E., Snell, R. L., et al. 2012, ApJ, 748, 37
Neufeld, D. A., Schilke, P., Menten, K. M., et al. 2006, A&A, 454, L37
Öberg, K. I., Linnartz, H., Visser, R., & van Dishoeck, E. F. 2009, ApJ, 693, 1209
O'Dell, C. R., & Wong, S. K. 1996, AJ, 111, 846
Ott, S. 2010, in ASP Conf. Ser. 434, Astronomical Data Analysis Software and Systems XIX, ed. Y. Mizuno, K. I. Morita, & M. Ohishi (San Francisco, CA: ASP), 139
Pellegrini, E. W., Baldwin, J. A., Ferland, G. J., Shaw, G., & Heathcote, S. 2009, ApJ, 693, 285
Pickett, H. M., Poynter, R. L., Cohen, E. A., et al. 1998, J. Quant. Spectrosc. Radiat. Transfer, 60, 883
Roelfsema, P. R., Helmich, F. P., Teyssier, D., et al. 2012, A&A, 537, A17
Schöier, F. L., van der Tak, F. F. S., van Dishoeck, E. F., & Black, J. H. 2005, A&A, 432, 369
Shaw, G., Ferland, G. J., Henney, W. J., et al. 2009, ApJ, 701, 677
Simon, R., Stutzki, J., Sternberg, A., & Winnewisser, G. 1997, A&A, 327, L9
Sternberg, A., & Dalgarno, A. 1995, ApJS, 99, 565
Walmsley, C. M., Natta, A., Oliva, E., & Testi, L. 2000, A&A, 364, 301
Westley, M. S., Baragiola, R. A., Johnson, R. E., & Baratta, G. A. 1995a, Nature, 373, 405
Westley, M. S., Baragiola, R. A., Johnson, R. E., & Baratta, G. A. 1995b, Planet. Space Sci., 43, 1311
Wyrowski, F., Schilke, P., Hofner, P., & Walmsley, C. M. 1997, ApJ, 487, L171
Young Owl, R. C., Meixner, M. M., Wolfire, M., Tielens, A. G. G. M., & Tauber, J. 2000, ApJ, 540, 886